Hindawi
Modelling and Simulation in Engineering
Volume 2024, Article ID 8637773, 13 pages
https://doi.org/10.1155/2024/8637773

Research Article

Theoretical Hydrodynamic Modeling of the Fluidized Bed Photoreactor (FBP) Using Computational Fluid Dynamics (CFD): Fluidization Conditions for TiO_2-CuO Immobilized on Beach Sand Granules

Ricardo Solano,[1] **Miguel Mueses**,[2] **and Adriana Herrera**[3]

[1]*Engineering Doctorate Program, Nanomaterials and Computer-Aided Process Engineering Research Group, University of Cartagena, 130015 Cartagena, Colombia*
[2]*School of Engineering, Department of Chemical Engineering, Modeling and Applications of Advanced Oxidation Technologies Research Group, Photocatalysis & Solar Photoreactors Engineering, University of Cartagena, 130015 Cartagena, Colombia*
[3]*School of Engineering, Department of Chemical Engineering, Nanomaterials and Computer Aided Process Engineering Research Group, University of Cartagena, 130015 Cartagena, Colombia*

Correspondence should be addressed to Ricardo Solano; rsolanop@unicartagena.edu.co

Received 16 October 2023; Revised 30 January 2024; Accepted 6 February 2024; Published 13 March 2024

Academic Editor: Chen Lin Soo

The flow regime is essential in the photoreactor's performance in pollutant degradation in the aqueous medium, especially in fluidized systems. Therefore, this study is focused on determining the fluidization conditions of a granular catalyst based on TiO_2-CuO nanoparticles (1 wt.% CuO) immobilized on beach sand granules using an FBP photoreactor. COMSOL Multiphysics 6.0 was employed for inlet velocities between 0.1 m/s and 1.0 m/s, mainly from the Reynolds averaged Navier–Stokes (RANS) turbulence model and the Stokes drag law. The results indicated that the average velocities in the annular section are much higher ($4.11u_t$ and $5.42u_t$) than the required particle terminal velocity. Moreover, the pressure contour lines revealed that these flow velocities do not represent excessive pressures in the concentric cylinders, with maximum gauge pressures of 740.52 Pa and 1310 Pa for inlet velocities $U_o = 0.75$ and 1.0 m/s, respectively. Finally, it was determined that the Reynolds number adjusted (Re_{pf}) values lower than or equal to 1.37×10^{-3} allow high fluidization after 2 seconds. This information makes it possible to adapt and assemble the FBP equipment for future photocatalytic evaluation.

1. Introduction

Commercial computational fluid dynamic (CFD) packages, such as COMSOL Multiphysics and ANSYS Fluent, have been successfully used in the simulation of advanced photochemical and nonphotochemical oxidation processes, specifically for the modeling of hydrodynamic [1–6], radiative [7–11], mass transfer [12–14], and kinetic [4, 15–18] phenomena, establishing the optimal values of typical dimensionless numbers, such as Reynolds (Re), Hatta (Ha), Schmidt (Sc), and Sherwood (Sh), among others, being helpful for the scaling process of this technology. According to the bibliometric study (2010-2023) carried out in this work using the Scopus database (http://www.scopus.com/), Figure 1(a) shows a growing interest of the international scientific community in topics related to the modeling and mathematical simulation of photoreactors used in advanced oxidation processes (AOPs). Moreover, leading researchers (Figure 1(b)) in the area were identified, among which Alfano, O. M.; Satuf, M. L.; Li Puma, G.; Marugán, J.; and Machuca-Martínez, F. stand out. Further, according to Figure 1(c), the National Natural Science Foundation of China and the Universidad Nacional del Litoral (Argentina) are the primary funding sponsors worldwide for research focused on reactor

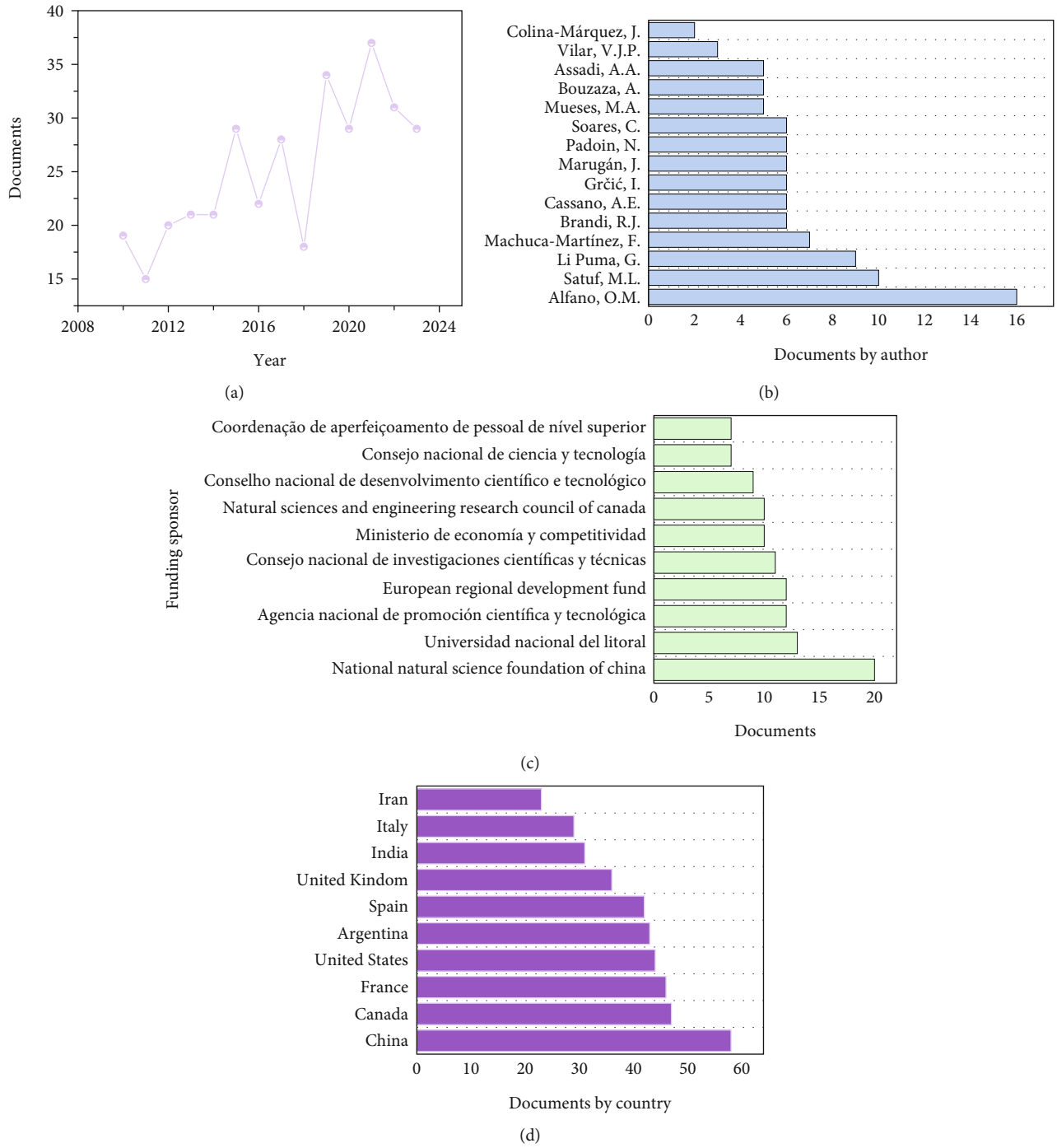

Figure 1: Continued.

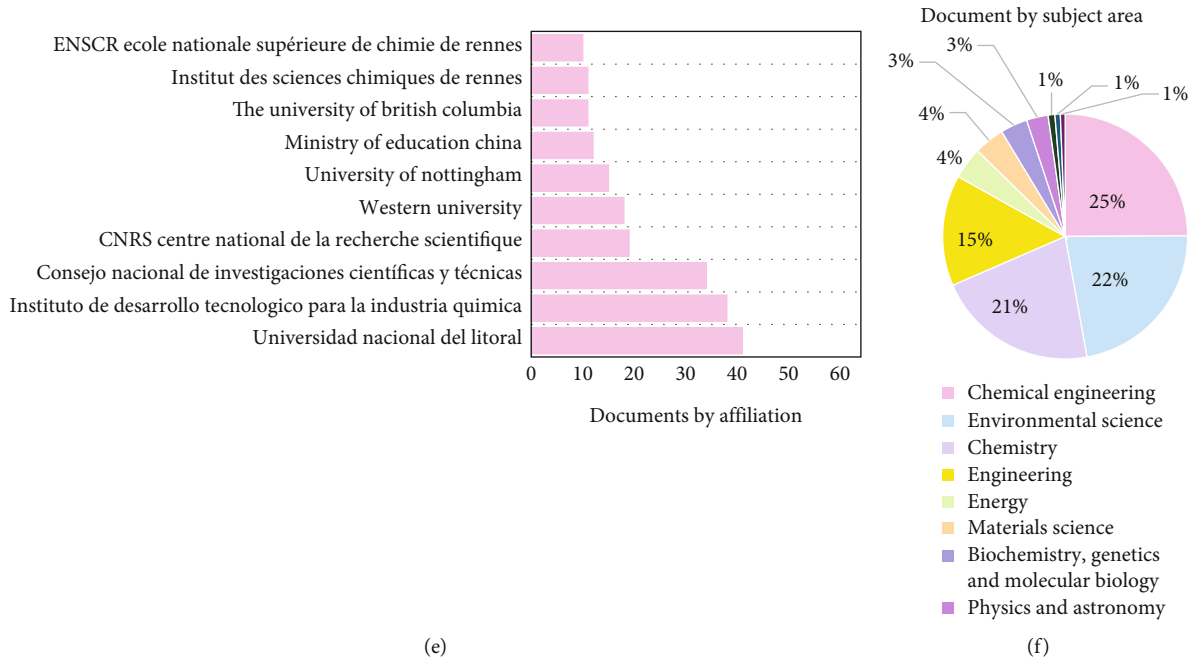

(e) (f)

Figure 1: Bibliometric analysis from Scopus: documents by (a) year, (b) author, (c) funding sponsor, (d) country, (e) affiliation, and (f) subject area. Search equation: (CFD OR "Computational fluid dynamics" OR Model∗ OR Simulation) AND ("Advanced oxidation processes" OR AOP OR photocatalysis) AND (Reactor OR Photoreactor).

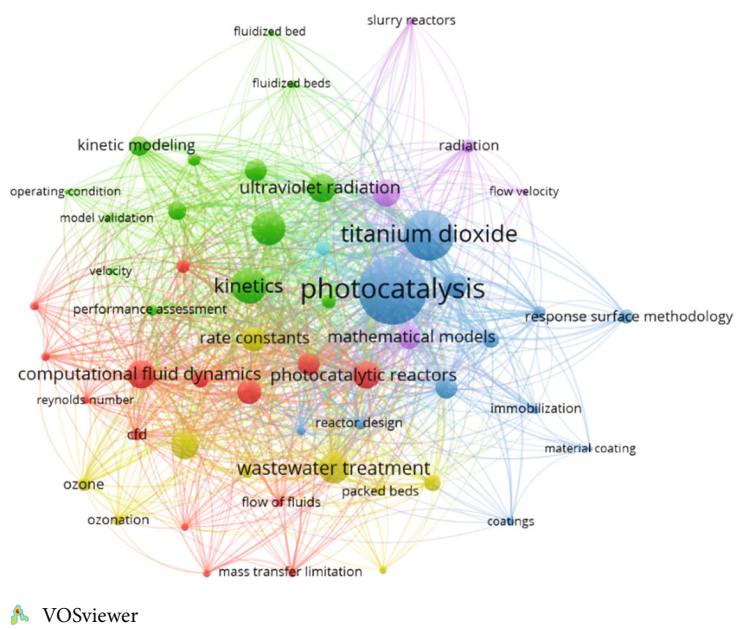

Figure 2: Map based on bibliometric data from VOSviewer 1.6.19.

modeling for AOPs, which agrees with the major countries' top (China, Canada, France, United States, Argentina, and Spain) and universities/affiliations, depicted in Figures 1(d) and 1(e), respectively. Besides, the most significant publications are scientific (85.4%) and review articles (5.9%) in chemical engineering, environmental sciences, and chemistry (see Figure 1(f)).

Furthermore, a map based on bibliographic data from Scopus was created in the VOSviewer (Figure 2), a software tool for constructing and visualizing bibliometric networks. This map confirmed the wide use of CFD programs and other modeling and simulation strategies for advanced oxidation processes, obtaining essential information, such as velocity and radiation fields, and kinetic models to study the mass transfer phenomena for both suspended and immobilized materials in packed and fluidized beds.

For example, Asgharian et al. [19] performed CFD modeling and validation in the COMSOL software of a

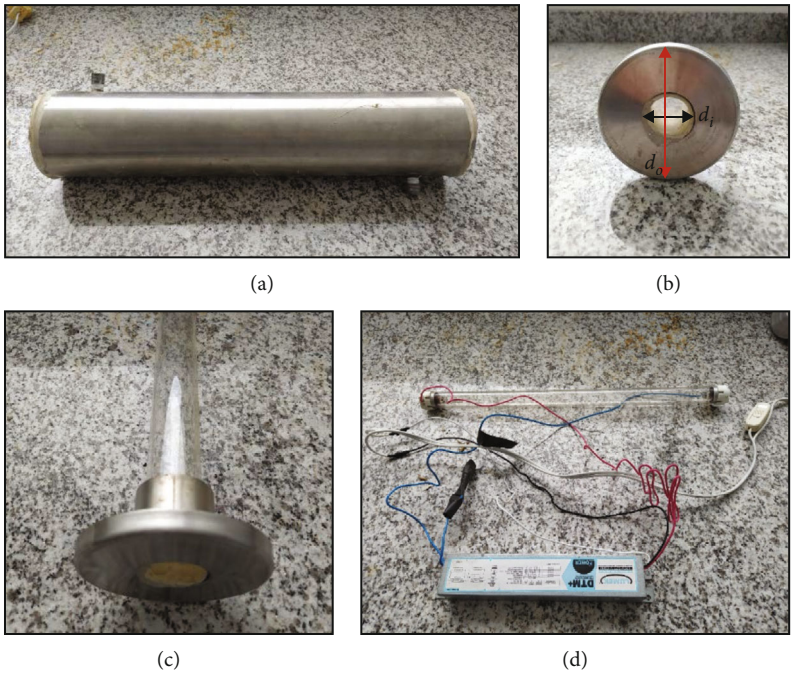

Figure 3: Fluidized bed annular photoreactor: (a) overview, (b) annular cross-section view, (c) borosilicate inner tube, and (d) UV-C lamp and power supply.

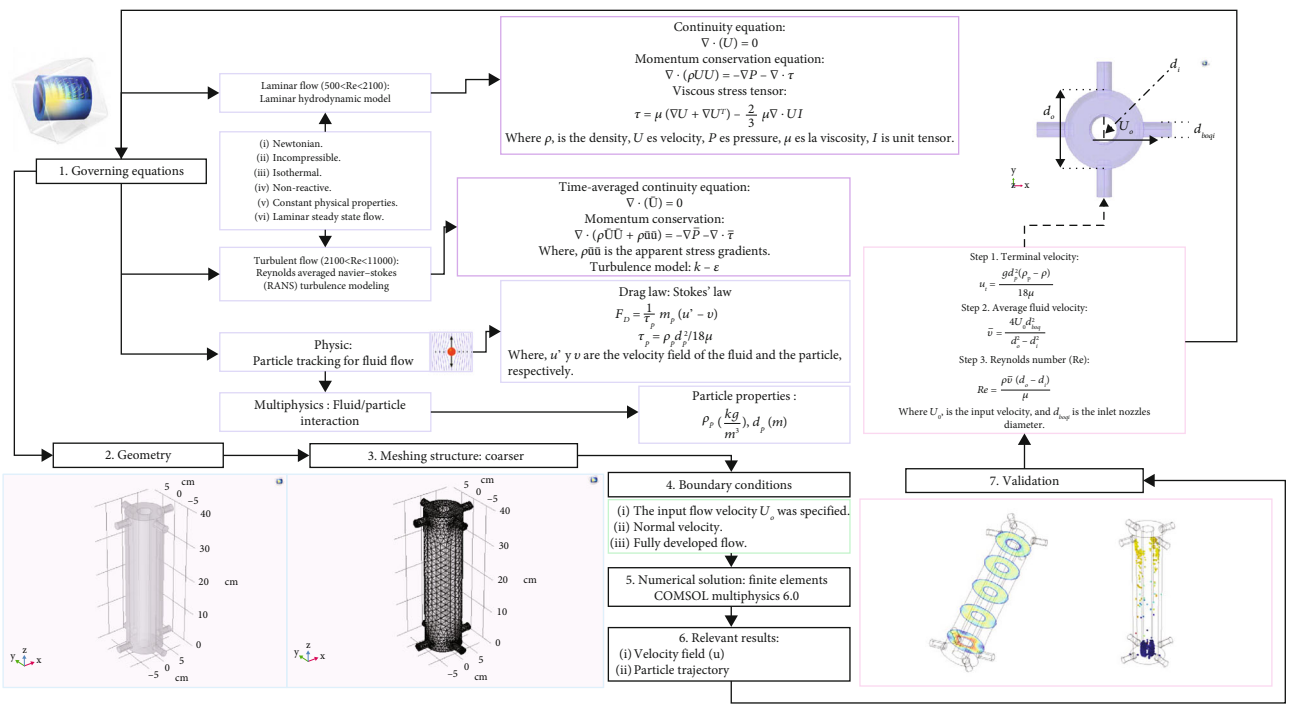

Figure 4: Methodological process for hydrodynamic modeling of fluidized bed annular photoreactor [1, 3, 4, 12, 24].

stirred tank photoreactor for photocatalytic tetracycline degradation using rGO/ZnO/Cu as a photocatalyst. For hydrodynamic modeling (pressure field: 4.44-0.06 Pa, velocity field: 0-0.16 m/s), the Reynolds-averaged Navier-Stokes turbulence model (RANS) and the continuity equation were used, while the phenomenon of mass transfer with a chemical reaction (concentration: 0.019-0.0225 mol/m^3) was studied using the mass conservation equation for each species and Fick's first diffusion law; on the other hand, for the radiation model (2.32-1.95 kW/m^2), the radiation transport equation (RTE) was considered. In a similar study, Ahmed et al. successfully modeled and validated ($R^2 = 0.998$) phenol degradation of waste and stormwater on a flat plate photocatalytic reactor with TiO_2 on a glass slide using the CFD

Table 1: Granular catalyst's physical properties and the dimensions and specifications of the fluidized bed annular photoreactor.

Granular photocatalyst		
Composition: TiO_2-CuO (1 wt.% CuO) immobilized on beach sand granules (0.04 g of catalyst/g of sand)	Granular size distribution: 0.212 mm-0.355 mm	Apparent density ($\rho_{apparent}$): 1450 kg/m^3
Fluidized bed annular photoreactor		
Dimensions: Length (40 cm) Internal diameter (3.8 cm) Outer diameter (10 cm) Nozzle's internal diameter (1.905 cm)	Materials: carbon steel/stainless steel alloy thickness (3 mm) Borosilicate tube thickness (2 mm)	UV-C lamp Length (43 cm) Power (15 W) Wavelength (253.7 nm)
Modeling parameters		
Turbulent flow ($k-\varepsilon$): Reference values: $P_{ref} = 1$ atm, $T_{ref} = 293.15$ K Turbulence model parameters: $C\varepsilon_1 = 1.44$, $C\varepsilon_2 = 1.92$, $C_\mu = 0.09$, $\sigma_k = 1$, $\sigma\varepsilon = 1.3$, $k_V = 0.41$, and $B = 5.2$	Particle tracking for fluid flow: bidirectionally coupled particle path: $d(m_p\mathbf{v})/dt = \mathbf{F_t}$ Maximum number of secondary particles: 10000	Fluid-particle interaction: $\partial F_v/\partial t = -\sum_{j=1}^{N_t} f_{rel} F_D \delta(\mathbf{r} - \mathbf{q}_j)$

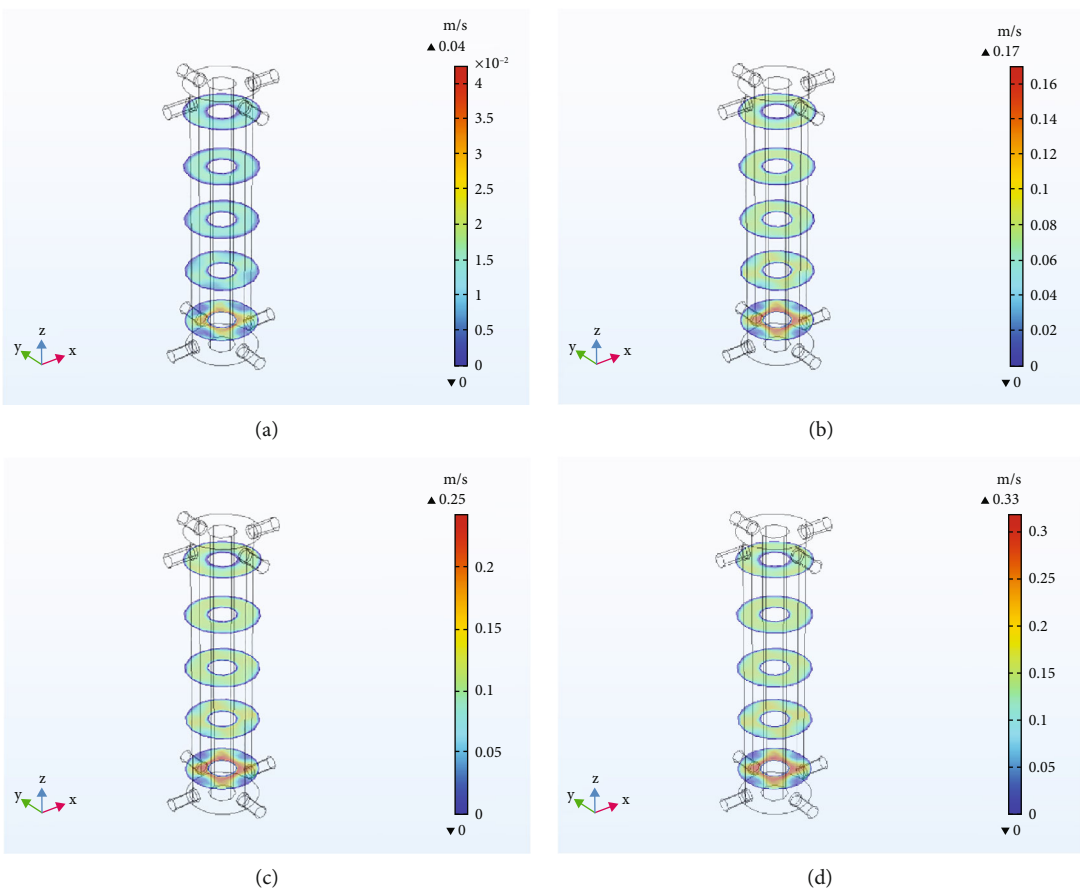

Figure 5: Velocity field (plane YZ) in the fluidized bed annular photoreactor for different U_o: (a) 0.1 m/s, (b) 0.5 m/s, (c) 0.75 m/s, and (d) 1.0 m/s.

code FLUENT in 3D. Also, Khataee et al. [20] reported photocatalytic ozonation for the anthelmintic drug degradation using ceramic-coated TiO_2 NPs through CFD simulation coupled with kinetic mechanisms.

This study represents a stage before the photocatalytic activity evaluation of the granular catalysts based on TiO_2-CuO immobilized on beach sand granules, whose objective is to determine the fluidization conditions in an annular photoreactor using the CFD software of COMSOL Multiphysics 6.0. The required flow regime analysis for fluidization represents an essential step in the concentric cylinder photoreactor's assembly before the photocatalytic evaluation of the granular catalyst with potential easy separation, reuse, and toxicological effect inhibition associated with

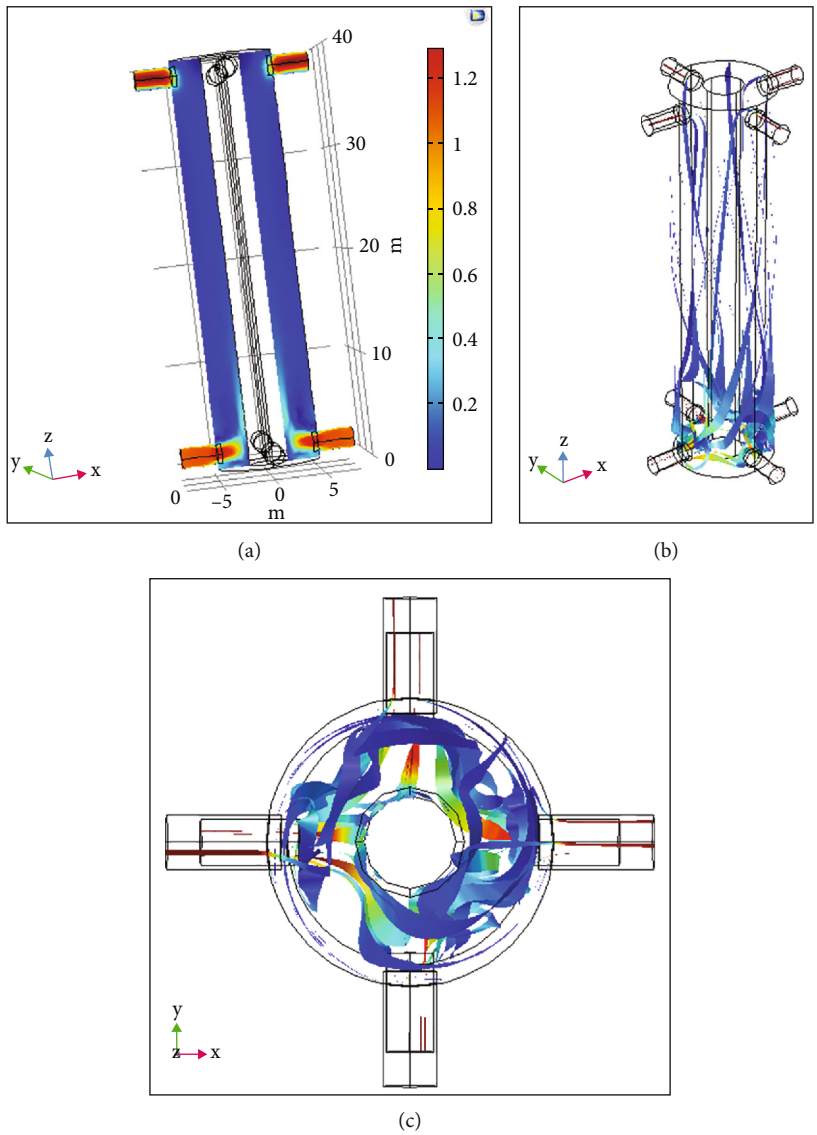

Figure 6: (a) Velocity field (plane ZX), (b) streamlines (YZ), and (c) streamlines (XY, bottom) in the annular photoreactor for U_o: 1.0 m/s.

nanomaterials remaining. Also, this research represents a prestudy to the photocatalytic degradation of metformin using TiO_2-CuO heterojunctions synthesized by green chemistry and immobilized on beach sand granules in a fluidized bed annular photoreactor. Moreover, these conditions have allowed the composite material fluidization to favor its dispersion and photoactivation throughout the entire flow reaction system through the annular section. Therefore, the experimental design for drug degradation in an aqueous medium has considered this flow rate range.

2. Methodology

2.1. Velocity Profiles in the Annular Region and Particle Trajectory. Hydrodynamic modeling was performed in the finite element analysis and resolution software COMSOL 6.0 (licensed through the University of Cartagena), following the stages described by Memon et al. [21]. Figure 3 describes each stage for generating the velocity profiles and estimating the trajectory of the particles dragged by the fluid flow from the physical model shown in Figure 4. The apparent density (ρ_{apparent}) of the granular photocatalyst was determined by the graduated cylinder method using the following equation [22]:

$$\rho_{\text{apparent}} = \frac{m_{\text{tot}}}{V_{\text{app}}}, \tag{1}$$

where m_{tot} is the total mass of the granular catalyst and V_{app} is the apparent volume including solids and internal pores. Besides, an intermediate size range was selected after the sieving process in an Orto Alresa machine (Model: VIBRO), corresponding to the fine sand type. Moreover, Table 1 summarizes the granular catalyst's physical properties, dimensions, and specifications of the fluidized bed annular photoreactor, and parameters considered in the fluidization conditions of the granular catalyst, which are

Table 2: CFD and calculated velocities for different inlet velocities.

Inlet velocity, U_o (m/s)	$\bar{v}_i^{CFD}/\bar{v}_i^{Cal}$ (m/s)	$f = \bar{v}_i^{CFD}/u_t^*$	Re number	RMSD/ADD
0.1	0.020/0.017	0.657	1029	0.0029/0.0025
0.5	0.085/0.084	2.793	2573	
0.75	0.125/0.127	4.107	7719	
1.0	0.165/0.169	5.421	10292	

*The terminal velocity ($u_t = 0.030$ m/s) was calculated for the maximum particle size (0.355 mm).

Table 3: Photoreactors' CFD modeling data for similar geometries from recent literature.

Photoreactor type/ CFD software	Specifications	Flow regime	Velocity profile*	Ref
Cylindrical UV-LED photoreactor/ ANSYS –Fluent	Aluminum/radius (3.67 cm), length (30 cm)	Turbulent (maximum velocity: 0.31 m/s)	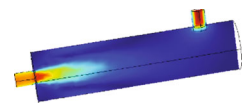	[37]
Annular photoreactor/ ANSYS -Fluent	External radius (5 cm), internal radius (2 cm), length (50 cm), wall thickness (0.5 cm), inlet tube diameter (2 cm), and exit tube diameter (3 cm)	Turbulent (maximum velocity: 0.5 m/s)	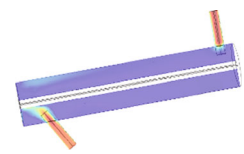	[5, 38]
Annular pilot plant reactor/OpenFOAM (*R*)	External radius (15 cm), internal radius (7 cm), length (50 cm), wall thickness (2.0 cm), inlet/outlet tube diameter (3 cm)	Laminar (maximum velocity: 0.05 m/s)	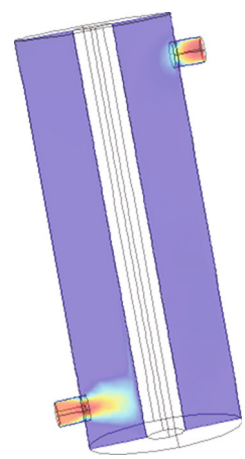	[39]

*The authors of this work illustrated the velocity profiles in COMSOL 6.0 from the reference report.

indispensable for hydrodynamic modeling. Furthermore, the immobilization process was performed using the two-step method of immersion/heat treatment, reported in a recent publication by our research group, which focuses on the optical, morphological, and structural characterization of TiO_2-CuO heterojunction nanoparticles synthesized by green chemistry supported on beach sand granules [23].

3. Results and Discussion

3.1. Velocity Field. The velocity fields (**u**) were modeled with up-flow for four input velocities ($U_o = 0.1$, 0.5, 0.75, and 1.0 m/s). These velocity profiles (plane *YZ*) are illustrated in Figures 5(a)–5(d). For all cases, maximum speeds are appreciated in the area where the four inlet nozzles direct the flow towards a direct impact with the external wall (see Figure 6(c)) of the borosilicate tube allowing the passage of UV radiation from the lamp. Furthermore, the continuity of the flow lines is observed, up to approximately half of the photoreactor for subsequent stabilization (see Figure 6(b)) with a piston-type flow regime in the annular region at the top of the photoreactor (see plane *ZX* for U_o: 1.0 m/s in Figure 6(a)).

The average velocity ($\bar{v}$, m/s) was calculated by applying the continuity equation; the flow regime was also determined. The values obtained were compared with the estimated data (see Table 2) from COMSOL CFD software using the standard deviation of the residuals (prediction errors) by root mean square deviation (RMSD, Equation (2)) and the average absolute deviation (AAD, Equation (3)) [25].

$$\mathrm{RMSD}\left(\bar{v}\right) = \sqrt{\sum_{i=1}^{N} \frac{\left(\bar{v}_i^{CFD} - \bar{v}_i^{Cal}\right)^2}{N}}, \quad (2)$$

$$\mathrm{ADD}\left(\bar{v}\right) = \frac{1}{N}\sum_{i=1}^{N}\left|\bar{v}_i^{CFD} - \bar{v}_i^{Cal}\right|. \quad (3)$$

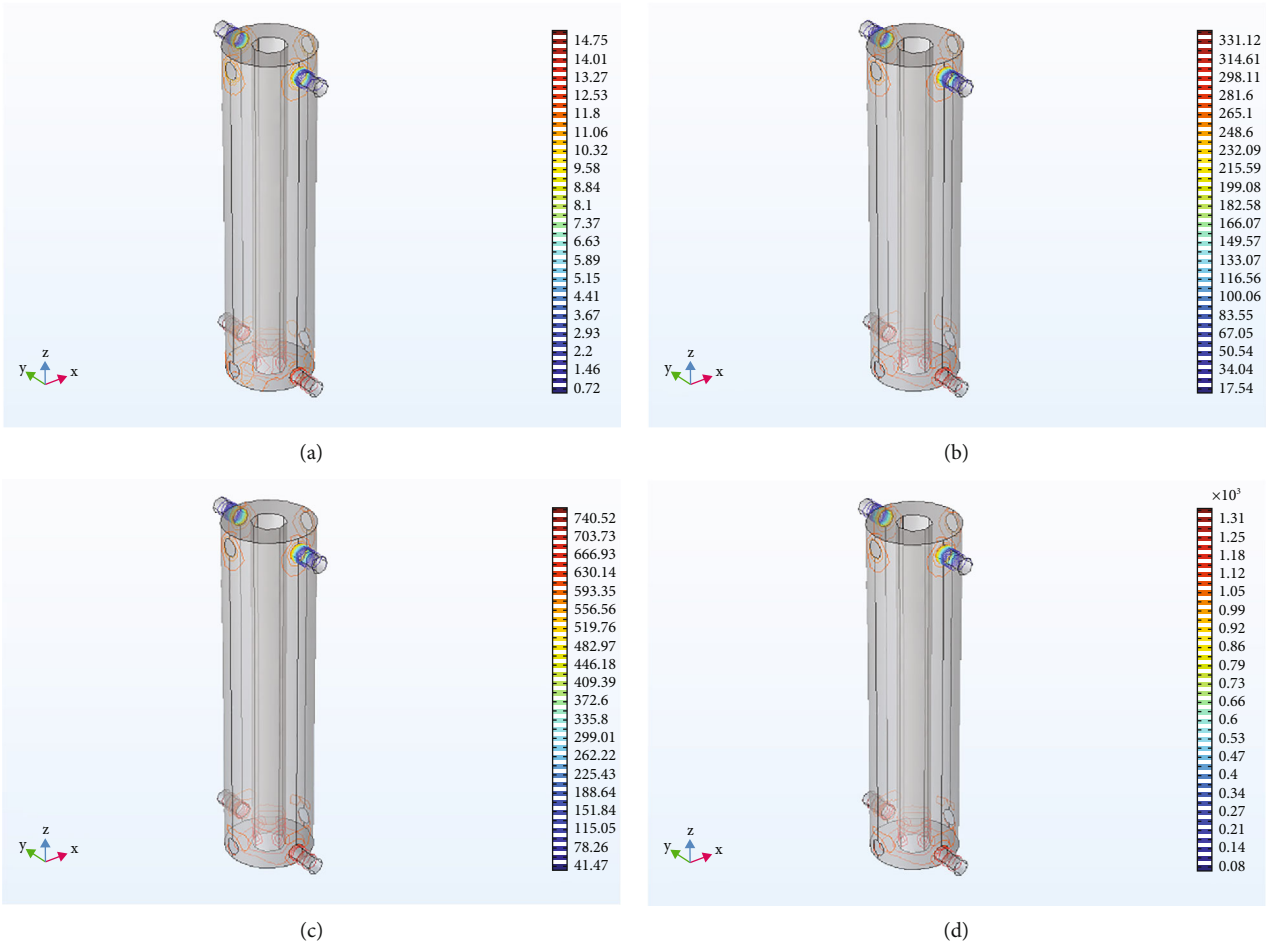

Figure 7: Pressure's contour lines in the fluidized bed annular photoreactor for different U_o: (a) 0.1 m/s, (b) 0.5 m/s, (c) 0.75 m/s, and (d) 1.0 m/s.

Both statistical indicators have values close to 0 (<0.003), which indicates that the CFD hydrodynamic model adequately predicts the velocity field. Table 3 presents a compilation of information relevant to the velocity profile obtained by CFD modeling for three tubular photoreactors reported in recent research. However, CFD modeling has been developed for other photocatalytic reactors, such as the raceway pond reactor [26], stirred tank [20], packing bed [27], compound parabolic collector [28, 29], parallel-channel microreactor [16], curved channel [30], photo impinging streams cyclone [31], cross-flow [32], flat plate [33], baffled flat-plate [34], and static mixer [35], among others. In other work, Liu et al. [36] have developed a CFD modeling in gas-liquid-solid mini-fluidized beds. However, the dragging of solid particles was caused by the air distribution at the photoreactor's bottom. The research in Table 3 corresponds to photoreactors' CFD modeling with similar geometries as the FBP proposed in this study without including solid particles' fluidization through the drag phenomenon.

3.2. Pressure Profile. The pressure's contour lines were modeled with up-flow for four input velocities ($U_o = 0.1$, 0.5, 0.75, and 1.0 m/s). These pressure profiles (plane YZ) are illustrated in Figures 7(a)–7(d). In these contour lines, maximum gauge pressures of 14.75 Pa, 331.12 Pa, 740.52 Pa, and 1310 Pa were identified at the bottom of the fluidized bed annular photoreactor for inlet velocities, $U_o = 0.1$, 0.5, 0.75, and 1.0 m/s, respectively; while the lowest pressures are in the discharge nozzles.

Most CFD studies of photoreactors do not report on pressure profiles; despite this, three recent publications were found that included this variable in their CFD analysis, as is the case of Asgharian et al. [19], who obtained the contour lines for pressure gauge inside a stirred tank photoreactor equipped with 8-blade backswept impeller for tetracycline degradation. These authors informed that after 0.5 min, the pressure increased and eventually reached about 4 Pa. Also, the pressure was negative behind the mixer blades and positive in front of them.

The research in Table 4 corresponds to the photoreactors' pressure profile obtained by CFD modeling with similar geometries but with a different orientation (horizontal) to the proposal in this study (vertical).

3.3. Particle's Trajectory. This section shows the particle trajectory results in the fluidized bed annular photoreactor for the four study velocities ($U_o = 0.1$, 0.5, 0.75, and 1.0 m/s), corresponding to $0.66u_t$, $2.79u_t$, $4.11u_t$, and $5.42u_t$,

Table 4: Photoreactors' pressure profile data obtained by CFD modeling for similar geometries.

Photoreactor type/CFD software	Specifications	Max/min gauge pressure (Pa)	Velocity profile*	Ref
Rotating annular VUV reactor/ANSYS	External radius (5 cm), internal radius (2 cm), length (50 cm), wall thickness (0.5 cm), inlet tube diameter (2 cm), and exit tube diameter (3 cm)	12.40/5.20	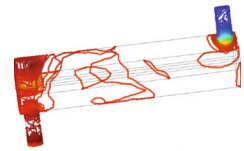 (Horizontal)	[40]
Bubble slurry photoreactor/COMSOL	Rectangle with a width of 5 cm and a length of 11 cm. Spargers with a 1 mm pore diameter are implemented at the reactor's bottom	1030/0.01	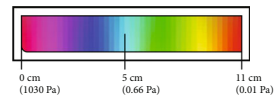 (Vertical)	[41]

*The authors of this work illustrated the pressure profiles from the reference report.

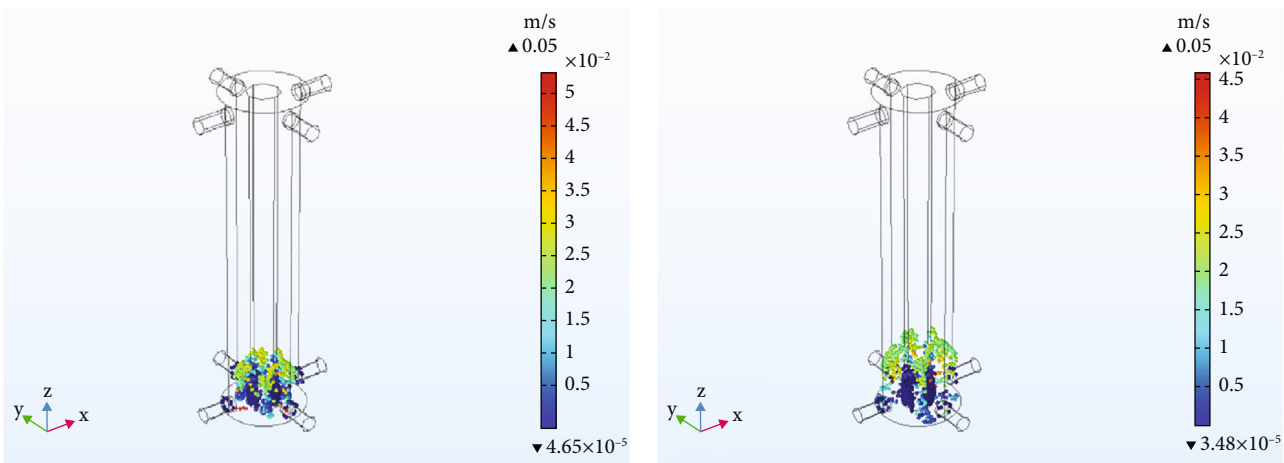

(a) (b)

Figure 8: Particle trajectory for TiO_2-CuO (1 wt.% CuO) synthesized by green chemistry and immobilized on beach sand granules (0.04 g of catalyst/g of sand) in the fluidized bed annular photoreactor: (a) 2 seconds and (b) 3 seconds for $U_o = 0.1$ m/s ($0.66u_t$).

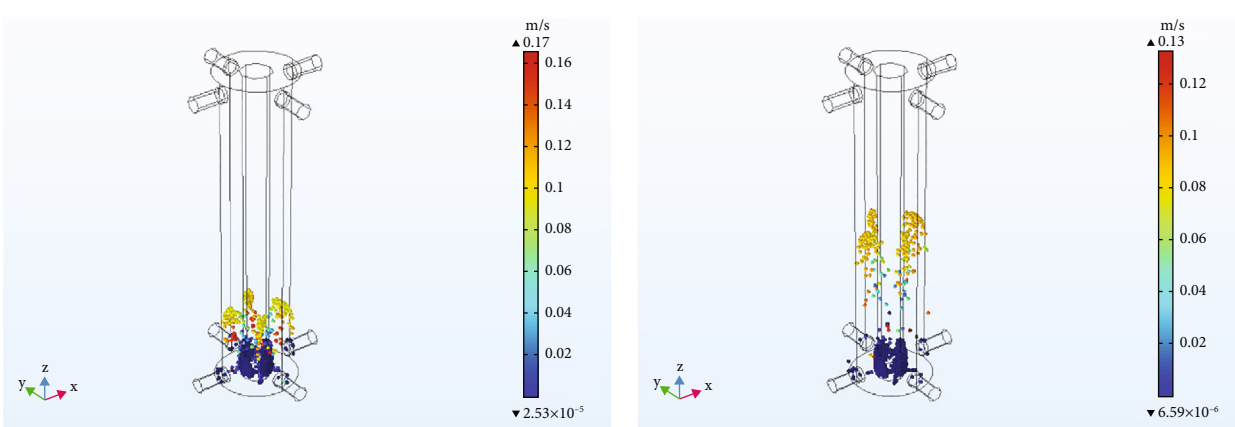

(a) (b)

Figure 9: Particle trajectory of granular catalyst in the fluidized bed annular photoreactor: (a) 0.8 seconds and (b) 2 seconds for $U_o = 0.5$ m/s ($2.79u_t$).

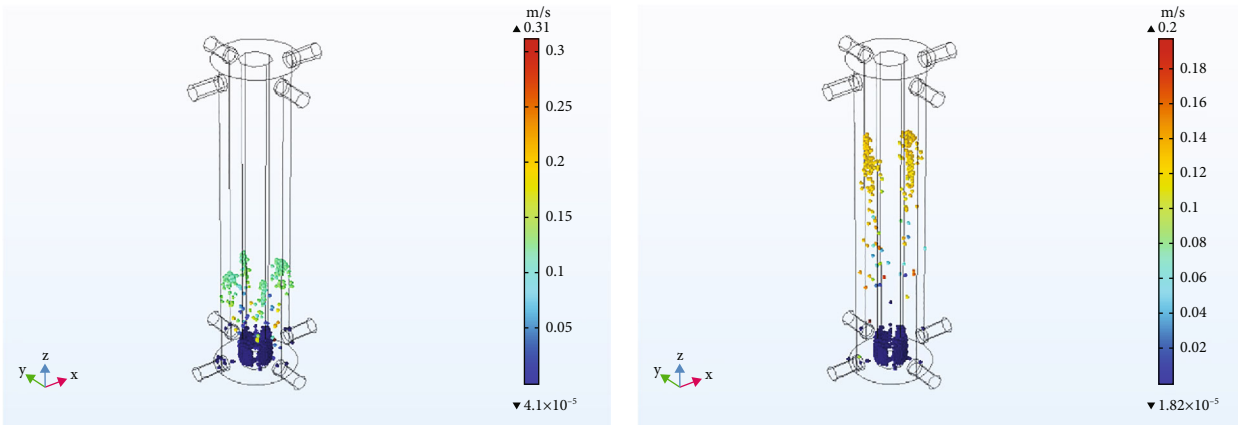

(a) (b)

Figure 10: Particle trajectory of granular catalyst in the fluidized bed annular photoreactor: (a) 0.8 seconds and (b) 2 seconds for $U_o = 0.75$ m/s ($4.11u_t$).

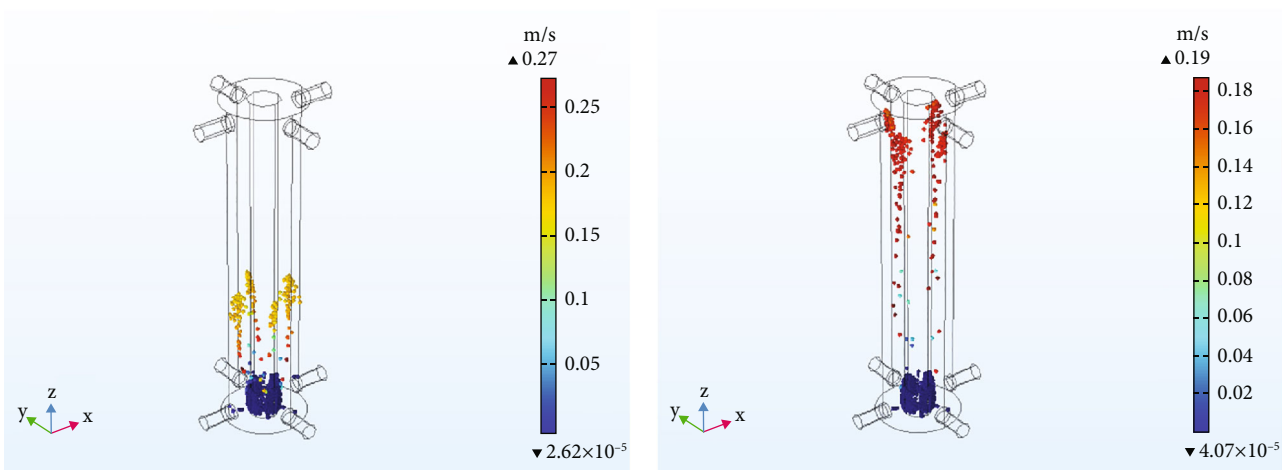

(a) (b)

Figure 11: Particle trajectory of granular catalyst in the fluidized bed annular photoreactor: (a) 0.8 seconds and (b) 2 seconds for $U_o = 1.0$ m/s ($5.42u_t$).

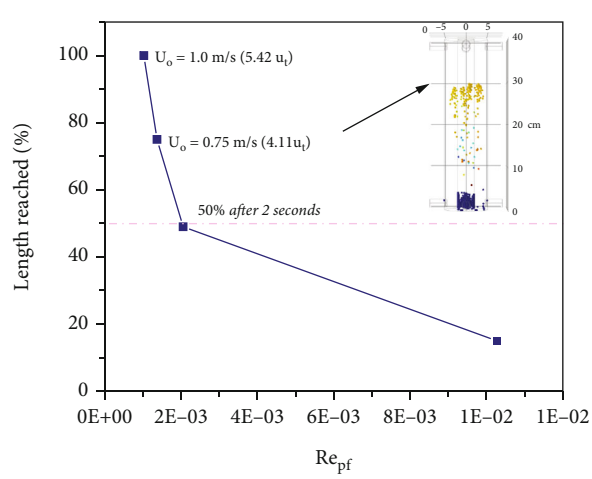

Figure 12: Length reached as a R_{pf} function after 2 seconds in the annular fluidized photoreactor.

respectively. In the case of $U_o = 0.1$ m/s ($0.66u_t$), the particles do not leave the bottom (see Figure 8) because the fluid's velocity is lower than the terminal velocity ($u_t = 0.030$ m/s). This phenomenon was reported by Picabea et al. [42], who found negligible fluidization for velocities below 0.021 m/s in a liquid-solid fluidized bed (LSFB) system with calcium alginate spheres. However, for velocities higher than terminal velocity ($2.79u_t$, $4.11u_t$, and $5.42u_t$), considerable fluidization is achieved due to drag, as shown in Figures 9–11, respectively. In a similar study, Abdulrahman et al. [43] demonstrated the influence of diameter (0.003 m, 0.004 m, and 0.006 m with a density of 2500 kg/m^3) of glass spheres and fluid velocity on fluidization velocity in a liquid-solid fluidized bed system; from results, authors informed that the expansion ratio is proportional to the liquid velocity and inversely proportional to the diameter of the beads.

Other research has also analyzed fluidized systems such as bubbling [44], droplet injection [45], and gas-liquid-solid flow [46]. Still, studies have not been focused on photocatalytic applications in vertical concentric cylindrical equipment.

To ensure the granular catalyst's fluidization, a potential scaling-up was found through dimensional analysis-Buckingham π theorem, a Reynolds number adjusted ($\mathrm{Re}_{\mathrm{pf}}$) (Equation (4)) to a liquid-solid fluidized system, which relates the particle's Reynolds number ($\mathrm{Re}_{\mathrm{pf}}$) [15] with the flow developed Reynolds number (Re_f) in the annular region for the average velocity ($\bar{\boldsymbol{v}}_{\boldsymbol{i}}^{\mathbf{CFD}}$).

$$\mathrm{Re}_{\mathrm{pf}} = \frac{\left(d_p^2\left(\rho_p - \rho\right)/18\mu\right)d_p}{\left(4U_0 d_{boqi}^2/d_o^2 - d_i^2\right)\left(d_o - d_i\right)}. \tag{4}$$

Besides, it is proposed to select the $\mathrm{Re}_{\mathrm{pf}}$ values (see Figure 12) that allow exceeding half the reactor's length after two seconds (2 s) since rapid fluidization of the heterogeneous photocatalytic system is required. This analysis indicates that the velocities are $U_o = 0.75$ m/s ($4.11u_t$) and $U_o = 1.0$ m/s ($5.42u_t$), i.e., a velocity field with an average value greater than 4.11 times the particle's terminal velocity.

4. Conclusions

In this research, the fluidized bed annular photoreactor's hydrodynamics was successfully modeled before the adaptation and assembly process for the photocatalytic evaluation of the granular photocatalyst based on TiO_2-CuO heterojunctions immobilized on beach sand granules. The results indicate that inlet velocities of $U_o = 0.75$ m/s and $U_o = 1.0$ m/s are required, generating average velocities in the annular section much higher than the particle terminal velocity, corresponding to $4.11u_t$ and $5.42u_t$, respectively. Moreover, contour lines were obtained for the gauge pressure in the concentric cylinders, with maximum gauge pressures of 14.75 Pa, 331.12 Pa, 740.52 Pa, and 1310 Pa at the photoreactor's bottom for inlet velocities $U_o = 0.1$, 0.5, 0.75, and 1.0 m/s, respectively. Finally, it was determined that Reynolds number adjusted ($\mathrm{Re}_{\mathrm{pf}}$) values lower than or equal to 1.37×10^{-3} allow high fluidization after 2 seconds, corresponding to a short time frame to ensure fluidization from the beginning of the pilot scale photoreactor operation. This information makes it possible to adapt and assemble the FBP equipment for the photocatalytic evaluation of the granular catalyst. Finally, the findings facilitated the identification of the best photoreactor configuration, the inlet velocities range to guarantee the fluidized regime, as well as the proposal of an adjusted dimensionless number for replication in studies operating conditions standardization in fluidized photoreactors for wastewater treatment by heterogeneous photocatalysis with reusable granular catalysts.

Data Availability

The data used to support the findings of this study are available from the corresponding author upon request.

Conflicts of Interest

The authors declare that they have no conflicts of interest.

Authors' Contributions

Ricardo Solano was responsible for the conceptualization, methodology, formal analysis, investigation, mathematical modeling, simulation, and writing—review and editing. Miguel Mueses was responsible for the conceptualization, writing—review and editing, supervision, validation, formal analysis, writing—original draft, and visualization. Adriana Herrera was responsible for the conceptualization, resources, writing—review and editing, supervision, funding, and acquisition.

Acknowledgments

The author received financial support for the research and publication of this article from Universidad de Cartagena. The authors also thank the research Vice-Rectory (University of Cartagena) for its financial through the call "Trámites de la apertura de planes de fortalecimiento para la obtención de recursos a los grupos de investigación, clasificados por el por el Ministerio de Ciencia, Tecnología e Innovación (MINCIENCIAS) que soportan la línea principal de investigación de un doctorado de la Universidad de Cartagena" (year 2021, according to Resolution 00680 (April 29, 2021) and Act of Initiation 007-2021). The authors are grateful to the Universidad de Cartagena for the facilities to develop this research and especially to the Environmental Modeling Research Group (Civil Engineering) for providing the COMSOL 6.0 license used in this research.

References

[1] G. C. Tedesco and P. B. Moraes, "Innovative design of a continuous flow photoelectrochemical reactor: hydraulic design, CFD simulation and prototyping," *Journal of Environmental Chemical Engineering*, vol. 9, no. 5, article 105917, 2021.

[2] R. Peralta, M. Moreira, and G. Li Puma, "CFD modeling of pharmaceuticals and CECs removal by UV/H2O2 process in

helical microcapillary photoreactors and evaluation of OH radical rate constants," *Chemical Engineering Journal*, vol. 415, article 128833, 2021.

[3] Y. S. Ignatenko, A. A. Gavrilov, and O. B. Bocharov, "On spiral turbulent flow in an annular concentric channel," *Journal of Physics Conference Series*, vol. 1867, article 012010, 2021.

[4] J. E. Duran, M. Mohseni, and F. Taghipour, "Modeling of annular reactors with surface reaction using computational fluid dynamics (CFD)," *Chemical Engineering Science*, vol. 65, no. 3, pp. 1201–1211, 2010.

[5] C. Casado, J. Marugán, R. Timmers, M. Muñoz, and R. van Grieken, "Comprehensive multiphysics modeling of photocatalytic processes by computational fluid dynamics based on intrinsic kinetic parameters determined in a differential photoreactor," *Chemical Engineering Journal*, vol. 310, pp. 368–380, 2017.

[6] S. Vanessa, D. M. Lima, N. Padoin, and C. Soares, "CFD analysis of a H2O2 UVC water treatment process in the annular FluHelik reactor," *Environmental Science and Pollution Research*, vol. 28, pp. 41224–41232, 2021.

[7] H. E. Whyte, A. Subrenat, C. Raillard, and V. Héquet, "Understanding the influence of media geometry on the degradation of acrylonitrile: experimental and CFD analysis," *Chemical Engineering Science*, vol. 209, article 115217, 2019.

[8] R. Peralta, M. Moreira, and G. L. Puma, "Multiphysics computational fluid-dynamics (CFD) modeling of annular photocatalytic reactors by the discrete ordinates method (DOM) and the six-flux model (SFM) and evaluation of the contaminant intrinsic kinetics constants," *Catalysis Today*, vol. 361, pp. 77–84, 2021.

[9] J. Moreno, C. Casado, and J. Marugán, "Improved discrete ordinate method for accurate simulation radiation transport using solar and LED light sources," *Chemical Engineering Science*, vol. 205, pp. 151–164, 2019.

[10] Y. Boyjoo, M. Ang, and V. Pareek, "Some aspects of photocatalytic reactor modeling using computational fluid dynamics," *Chemical Engineering Science*, vol. 101, pp. 764–784, 2013.

[11] F. C. Moreira, E. Bocos, A. G. F. Faria et al., "Selecting the best piping arrangement for scaling-up an annular channel reactor: an experimental and computational fluid dynamics study," *Science of the Total Environment*, vol. 667, pp. 821–832, 2019.

[12] M. I. Jaramillo-gutiérrez, M. I. Carreño-lizcano, and J. O. Ruiz, "Design, mathematical modelling, and numerical simulation of a novel tubular photoelectrochemical reactor and experimental validation by residence time distribution and mass transfer coefficients," *Chemical Engineering Journal*, vol. 386, article 123895, 2020.

[13] S. Zhang, J. Zhang, J. Sun, and Z. Tang, "Capillary microphotoreactor packed with TiO2-coated glass beads: an efficient tool for photocatalytic reaction," *Chemical Engineering and Processing*, vol. 147, article 107746, 2020.

[14] M. Malayeri, C. Lee, F. Haghighat, and L. Klimes, "Modeling of gas-phase heterogeneous photocatalytic oxidation reactor in the presence of mass transfer limitation and axial dispersion," *Chemical Engineering Journal*, vol. 386, article 124013, 2020.

[15] J. A. Lara-ramos, J. Diaz-angulo, and F. Machuca-martínez, "Use of modified flotation cell as ozonation reactor to minimize mass transfer limitations," *Chemical Engineering Journal*, vol. 405, article 126978, 2021.

[16] A. Yusuf and G. Palmisano, "Three-dimensional CFD modelling of a photocatalytic parallel-channel microreactor," *Chemical Engineering Science*, vol. 229, article 116051, 2021.

[17] N. Singh, M. K. Das, R. Gautam, A. Ramteke, and P. Rajamani, "Assessment of intermittent exposure of zinc oxide nanoparticle (ZNP)–mediated toxicity and biochemical alterations in the splenocytes of male Wistar rat," *Environmental Science and Pollution Research*, vol. 26, no. 32, pp. 33642–33653, 2019.

[18] J. Kumar and A. Bansal, "Photocatalytic degradation in annular reactor: modelization and optimization using computational fluid dynamics (CFD) and response surface methodology (RSM)," *Journal of Environmental Chemical Engineering*, vol. 1, no. 3, pp. 398–405, 2013.

[19] M. Asgharian, B. Khoshandam, M. Mehdipourghazi, and N. Keramati, "Photocatalytic degradation of tetracycline in a stirred tank: computational fluid dynamic modeling and data validation," *Reaction Kinetics, Mechanisms and Catalysis*, vol. 134, no. 1, pp. 553–568, 2021.

[20] A. Khataee, M. E. Farshchi, M. Fathinia, and H. Aghdasinia, "Photocatalytic ozonation process for degradation of an anthelmintic drug using ceramic coated TiO2 NPs: CFD simulation coupling with kinetic mechanisms," *Process Safety and Environment Protection*, vol. 141, pp. 37–48, 2020.

[21] A. A. Memon, M. A. Memon, K. Bhatti et al., "Modelling and simulation of fluid flow through a circular cylinder with high Reynolds number: a COMSOL Multiphysics study," *Journal of Mathematics*, vol. 2022, Article ID 5282980, 9 pages, 2022.

[22] P. Basu, "Biomass characteristics," in *Biomass Gasification, Pyrolysis and Torrefaction*, pp. 49–91, Academic Press, Boca Raton, Third edition, 2018.

[23] R. Solano, D. Maestre, M. Mueses, and A. Herrera, "TiO2-CuO heterojunction nanoparticles synthesized by green chemistry supported on beach sand granules: optical, morphological and structural characterization," *Nano-Structures and Nano-Objects*, vol. 35, article 101024, 2023.

[24] M. S. Ramsey, *Practical Wellbore Hydraulics and Hole Cleaning*, Gulf Professional Publishing, Oxford, 2019.

[25] J. Pan, X. Li, W. Zhang, W. Cui, Z. Zhou, and D. Liu, "Isobaric vapour-liquid equilibrium for binary systems of ethyl iodide with ethanol, propionic acid and ethyl propionate at 101.3 kPa," *The Journal of Chemical Thermodynamics*, vol. 132, pp. 23–28, 2019.

[26] R. P. M. Moreira, A. C. Reina, P. S. Molina, J. A. S. Pérez, and G. L. Puma, "Computational fluid dynamics (CFD) modeling of removal of contaminants of emerging concern in solar photo-Fenton raceway pond reactors," *Chemical Engineering Journal*, vol. 413, article 127392, 2020.

[27] K. Tong, L. Yang, and X. Du, "Modelling of TiO2-based packing bed photocatalytic reactor with Raschig rings for phenol degradation by coupled CFD and DEM," *Chemical Engineering Journal*, vol. 400, article 125988, 2020.

[28] C. Nchikou, J. Á. Loredo-Medrano, A. Hernández-Ramírez, J. Á. Colina-Marquez, and M. Á. Mueses, "Estimation of the radiation field for CPC photocatalytic reactors using a novel six-flux model in two dimensions (SFM-2D)," *Journal of Environmental Chemical Engineering*, vol. 9, no. 6, article 106392, 2021.

[29] D. Wang, M. A. Mueses, J. A. C. Márquez et al., "Engineering and modeling perspectives on photocatalytic reactors for water treatment," *Water Research*, vol. 202, p. 117421, 2021.

[30] D. B. Lira, H. G. Riella, N. Padoin, and C. Soares, "Fluid dynamics and mass transfer in curved reactors: a CFD study on dean flow effects," *Journal of Environmental Chemical Engineering*, vol. 10, no. 5, article 108304, 2022.

[31] S. J. Royaee, M. Sohrabi, and A. Shafeghat, "Wastewater treatment using photo-impinging streams cyclone reactor: computational fluid dynamics and kinetics modeling," *Korean Journal of Chemical Engineering*, vol. 31, no. 2, pp. 240–247, 2014.

[32] M. Moghaddami, A. Jalali, P. Behnamghader, and M. Raisee, "Effect of vortex shedding on the performance of cross-flow UV-H2O2 photoreactors," *Chemical Engineering and Processing*, vol. 166, article 108471, 2021.

[33] S. Ahmed, M. G. Rasul, M. A. Sattar, and M. I. Jahirul, "Phenol degradation of waste and stormwater on a flat plate photocatalytic reactor with TiO2 on glass slide: an experimental and modelling investigation," *Journal of Water Process Engineering*, vol. 47, article 102769, 2022.

[34] J. S. Devia-orjuela, L. A. Betancourt-buitrago, and F. Machuca-martinez, "CFD modeling of a UV-A LED baffled flat-plate photoreactor for environment applications: a mining wastewater case," *Environmental Science and Pollution Research*, vol. 26, no. 5, pp. 4510–4520, 2019.

[35] D. Gholami, S. Shahbazi, S. Mosleh et al., "In situ growth of CuFeS2/CuS bridged heterojunction catalyst with mixed redox-couple cations for excellent photocatalytic degradation of organophosphate insecticide: CFD and DFT modeling," *Chemical Engineering Journal*, vol. 461, no. 2022, article 141950, 2023.

[36] Y. X. Liu, L. T. Zhu, Z. H. Luo, and J. X. Tang, "Effect of spatial radiation distribution on photocatalytic oxidation of methylene blue in gas-liquid-solid mini-fluidized beds," *Chemical Engineering Journal*, vol. 370, pp. 1154–1168, 2019.

[37] A. S. Kooshan, A. Jalali, and S. F. Chini, "Performance evaluation of point-of-use UVC-LED water disinfection photoreactors using CFD and response surface methodology," *Journal of Water Process Engineering*, vol. 46, article 102545, 2022.

[38] H. Yan, M. Luo, Q. Chen, T. Jeong, J. Zhang, and L. Wang, "Efficacy and mechanism of chemical-free VUV/UV process for oxytetracycline degradation: continuous-flow experiment and CFD modeling," *Chemical Engineering Journal Advances*, vol. 4, article 100059, 2020.

[39] C. M. Venier, L. O. Conte, M. Pérez-Moya, M. Graells, N. M. Nigro, and O. M. Alfano, "A CFD study of an annular pilot plant reactor for paracetamol photo-Fenton degradation," *Chemical Engineering Journal*, vol. 410, article 128246, 2021.

[40] M. Luo, W. Xu, X. Kang, K. Ding, and T. Jeong, "Computational fluid dynamics modeling of rotating annular VUV/UV photoreactor for water treatment," *Processes*, vol. 9, no. 1, p. 79, 2021.

[41] A. Asadi, A. Larimi, Z. Jiang, and A. Naderifar, "Modeling and simulation of photocatalytic CO2 reduction into methanol in a bubble slurry photoreactor," *Chemical Engineering Science*, vol. 263, article 118078, 2022.

[42] J. Picabea, M. Maestri, M. Cassanello et al., "Validation of CFD-DEM simulation of a liquid–solid fluidized bed by dynamic analysis of time series," *Particuology*, vol. 68, pp. 75–87, 2022.

[43] A. A. Abdulrahman, O. S. Mahdy, L. S. Sabri et al., "Experimental investigation and computational fluid dynamic simulation of hydrodynamics of liquid–solid fluidized beds," *ChemEngineering*, vol. 6, no. 3, p. 37, 2022.

[44] N. F. Nthatisi and A. F. Van Der Merwe, "Computational fluid dynamics (CFD) modelling of the effect of distributor plate geometry in the bubbling fluidized bed reactor," *South African Journal of Chemical Engineering*, vol. 43, pp. 46–59, 2023.

[45] L. Zhu, Z. Zhao, C. Liu et al., "CFD-DEM simulations of a fluidized bed with droplet injection: effects on flow patterns and particle behavior," *Advanced Powder Technology*, vol. 34, no. 1, article 103897, 2023.

[46] H. Pan, X. Z. Chen, X. F. Liang, L. T. Zhu, and Z. H. Luo, "CFD simulations of gas-liquid-solid flow in fluidized bed reactors - a review," *Powder Technology*, vol. 299, pp. 235–258, 2016.